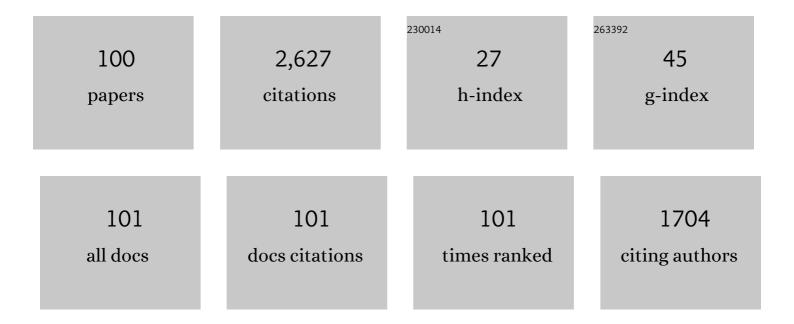
## Hao Chen

List of Publications by Year in descending order

Source: https://exaly.com/author-pdf/1949706/publications.pdf Version: 2024-02-01



#	Article	IF	CITATIONS
1	Phase Field Modeling of Austenite Decomposition and Formation in Steels: An Overview. , 2022, , 527-540.		0
2	Revealing the influence of Mo addition on interphase precipitation in Ti-bearing low carbon steels. Acta Materialia, 2022, 223, 117475.	3.8	22
3	Temperature dependence of carbon deposits within oxide scale on CrMoV steel in atmospheric and supercritical CO2. Corrosion Science, 2022, 195, 109979.	3.0	2
4	Quantitative evaluations of improved surface integrity in ultrasonic rolling process for selective laser melted in-situ TiB2/Al composite. Journal of Manufacturing Processes, 2022, 77, 412-425.	2.8	10
5	Chemical heterogeneity enables austenite stabilization in a Si-/Al-free Fe-0.2C-2Mn steel. Scripta Materialia, 2022, 218, 114822.	2.6	6
6	Transformation and Twinning-Induced Plasticity Effect in a Novel Heterogeneous Microstructural Medium-Mn Steel Processed by ART Annealing. Jom, 2022, 74, 2826-2837.	0.9	2
7	Fundamentals and application of solid-state phase transformations for advanced high strength steels containing metastable retained austenite. Materials Science and Engineering Reports, 2021, 143, 100590.	14.8	100
8	Critical role of Lüders banding in hydrogen embrittlement susceptibility of medium Mn steels. Scripta Materialia, 2021, 190, 32-37.	2.6	24
9	Atomistic insight into hydrogen trapping at MC/BCC-Fe phase boundaries: The role of local atomic environment. Acta Materialia, 2021, 208, 116744.	3.8	36
10	Phase-Field Modeling of Hydrogen Diffusion and Trapping in Steels. Acta Metallurgica Sinica (English) Tj ETQqO C	) 0 <sub>[</sub> gBT /O	verlock 10 T
11	Flash annealing yields a strong and ductile medium Mn steel with heterogeneous microstructure. Scripta Materialia, 2021, 198, 113819.	2.6	46
12	Chemical heterogeneity enhances hydrogen resistance in high-strength steels. Nature Materials, 2021, 20, 1629-1634.	13.3	83
13	Unraveling the effects of Nb interface segregation on ferrite transformation kinetics in low carbon steels. Acta Materialia, 2021, 215, 117081.	3.8	25
14	Revealing carbide precipitation effects and their mechanisms during quenching-partitioning-tempering of a high carbon steel: Experiments and Modeling. Acta Materialia, 2021, 217, 117176.	3.8	21
15	Effect of CO2 gas pressure on composition, growth rate, and structure of duplex oxide formed on 9Cr steel at 550 ŰC. Corrosion Science, 2020, 163, 108252.	3.0	13
16	Understanding microstructure-evolution-dependent fracture behaviors in pearlitic steels. Journal of Iron and Steel Research International, 2020, 27, 334-341.	1.4	2

17	Enhancement of cyclic oxidation resistance and effect of transition oxides on wear mechanism of yttrium plus aluminium modified tribaloy T-900 alloy. Corrosion Science, 2020, 163, 108283.	3.0	5
18	Hot corrosion behaviour of yttrium and aluminium modified wear resistance coating alloy in mixed sulphate at 900†°C. Corrosion Science, 2020, 165, 108369.	3.0	20

2

#	Article	IF	CITATIONS
19	On the role of chemical heterogeneity in phase transformations and mechanical behavior of flash annealed quenching & partitioning steels. Acta Materialia, 2020, 201, 266-277.	3.8	47
20	Incomplete carbon partitioning during quenching and partitioning of Fe–C–Mn–Si steels: Modeling and experimental validations. Acta Materialia, 2020, 200, 597-607.	3.8	21
21	Carbon depositions within the oxide scale and its effect on the oxidation behavior of low alloy steel in low (0.1†MPa), sub-(5†MPa) and supercritical (10†MPa) CO2 at 550°C. Corrosion Science, 2020, 177, 108950.	3.0	12
22	A comparative study on intrinsic mobility of incoherent and semicoherent interfaces during the austenite to ferrite transformation. Scripta Materialia, 2020, 188, 59-63.	2.6	20
23	How chemical boundary engineering can produce cheap, ultra-strong steels. Proceedings of the Institution of Civil Engineers: Civil Engineering, 2020, 173, 102-102.	0.3	2
24	A fully biodegradable and self-electrified device for neuroregenerative medicine. Science Advances, 2020, 6, .	4.7	88
25	Microstructure of a Ti–50Âwt% Ta alloy produced via laser powder bed fusion. Acta Metallurgica Sinica (English Letters), 2020, 33, 981-990.	1.5	13
26	Chemical boundary engineering: A new route toward lean, ultrastrong yet ductile steels. Science Advances, 2020, 6, eaay1430.	4.7	120
27	Microstructural Instability and Precipitation Behaviors of Intermetallic Phases in a Nb-Containing CoNi-Based Superalloy. Metallurgical and Materials Transactions A: Physical Metallurgy and Materials Science, 2020, 51, 2495-2508.	1.1	3
28	Correlation of creep fracture lifetime with microstructure evolution and cavity behaviors in G115 martensitic heat-resistant steel. Materials Science & Engineering A: Structural Materials: Properties, Microstructure and Processing, 2020, 788, 139468.	2.6	25
29	Kinetic transitions and Mn partitioning during austenite growth from a mixture of partitioned cementite and ferrite: Role of heating rate. Journal of Materials Science and Technology, 2020, 49, 70-80.	5.6	31
30	Revealing the effect of grain boundary segregation on Li ion transport in polycrystalline anti-perovskite Li <sub>3</sub> ClO: a phase field study. Physical Chemistry Chemical Physics, 2020, 22, 3030-3036.	1.3	30
31	Thermal and mechanical properties of ferroelastic RENbO4 (REÂ=ÂNd, Sm, Gd, Dy, Er, Yb) for thermal barrier coatings. Scripta Materialia, 2020, 180, 51-56.	2.6	45
32	A New Kinetic Mode During the Austenite-to-Ferrite Transformation in Fe–Mn and Fe–Mn–Mo Alloys. Acta Metallurgica Sinica (English Letters), 2020, 33, 975-980.	1.5	3
33	A two-set order parameters phase-field modeling of crack deflection/penetration in a heterogeneous microstructure. Computer Methods in Applied Mechanics and Engineering, 2019, 347, 1085-1104.	3.4	26
34	Oxidation behavior and lifetime prediction of three commercial alloys used in power plants at 550°C in CO2 environment. Journal of Iron and Steel Research International, 2019, 26, 898-908.	1.4	8
35	Coordination of Pre-oxidation Time and Temperature for a Better Corrosion Resistance to CO2 at 550°C. Oxidation of Metals, 2019, 91, 657-675.	1.0	4
36	Plastic deformation behaviors and mechanical properties of advanced single crystalline CoNi-base superalloys. Materials Science & Engineering A: Structural Materials: Properties, Microstructure and Processing, 2019, 748, 267-274.	2.6	16

#	Article	IF	CITATIONS
37	Microstructure and high-temperature mechanical properties of second-phase enhanced Mo-La2O3-ZrC alloys post-treated by cross rolling. Journal of Alloys and Compounds, 2019, 796, 167-175.	2.8	26
38	Stabilizing austenite via a core-shell structure in the medium Mn steels. Scripta Materialia, 2019, 166, 68-72.	2.6	40
39	Comparative cyclic oxidation behaviour and effect of oxides on hardness of wear resistance coating alloys T-401 and T-900. Journal of Iron and Steel Research International, 2019, 26, 1069-1079.	1.4	3
40	Improving the ductility of ultrahigh-strength medium Mn steels via introducing pre-existed austenite acting as a "reservoir―for Mn atoms. Materials Science & Engineering A: Structural Materials: Properties, Microstructure and Processing, 2019, 749, 235-240.	2.6	26
41	Nanoprecipitation-suppressed ferrite transformation (γ →â€Î±) during tempering in a medium‑manganese s Scripta Materialia, 2019, 162, 391-396.	steel. 2.6	11
42	Comparison of Microstructural Evolution of Oxides Formed on F91 Martensitic Steel Upon Breakaway Oxidation at 700°C in Air and CO2. Oxidation of Metals, 2019, 91, 463-482.	1.0	1
43	A new treatment of alloying effects on migrating interfaces in Fe-X alloys. Scripta Materialia, 2019, 162, 44-48.	2.6	7
44	Abnormal Anisotropic Dilatation During Bainitic Transformation of Ausformed Austenite. Metallurgical and Materials Transactions A: Physical Metallurgy and Materials Science, 2019, 50, 540-546.	1.1	10
45	Thermo-kinetic design of retained austenite in advanced high strength steels. Acta Materialia, 2018, 152, 288-299.	3.8	40
46	Effect of strain on the intrinsic stacking fault energy of fcc Co: a first-principles study. Journal of Materials Science, 2018, 53, 10217-10230.	1.7	9
47	Effect of pre-existed austenite on austenite reversion and mechanical behavior of an Fe-0.2C-8Mn-2Al medium Mn steel. Acta Materialia, 2018, 147, 59-69.	3.8	137
48	Effect of Al on martensite tempering: comparison with Si. Journal of Materials Science, 2018, 53, 6951-6967.	1.7	23
49	Pre-oxidation Effect on Oxidation Behavior of F91 in Carbon Dioxide at 550°C. Oxidation of Metals, 2018, 90, 317-335.	1.0	8
50	Effect of solute segregation on the intrinsic stacking fault energy of Co-based binary alloys: A first-principles study. Journal of Alloys and Compounds, 2018, 748, 328-337.	2.8	19
51	Effects of co-addition of Ni and Al on precipitation evolution and mechanical properties of Fe-Cu alloy. Materials Science & Engineering A: Structural Materials: Properties, Microstructure and Processing, 2018, 723, 279-286.	2.6	23
52	High-Temperature Oxidation Behavior of CrMoV, F91 and Mar-M247 Superalloys Exposed to Laboratory Air at 550°C. Oxidation of Metals, 2018, 90, 401-419.	1.0	5
53	Decelerated Coarsening of (Ti, Mo)C Particles with a Core–Shell Structure in Austenite of a Ti-Mo-Bearing Steel. Metallurgical and Materials Transactions A: Physical Metallurgy and Materials Science, 2018, 49, 1455-1459.	1.1	16
54	Elucidating the effect of Mn partitioning on interface migration and carbon partitioning during Quenching and Partitioning of the Fe-C-Mn-Si steels: Modeling and experiments. Acta Materialia, 2018, 144, 666-678.	3.8	60

#	Article	IF	CITATIONS
55	Computational thermodynamic and first-principles calculation of stacking fault energy on ternary Co-based alloys. Computational Materials Science, 2018, 143, 112-117.	1.4	31
56	Solubility and Anisotropic Migration Behaviors of Helium in bcc Iron Under Strain. Acta Metallurgica Sinica (English Letters), 2018, 31, 199-207.	1.5	2
57	Microstructural evolution and hardness of a heat resistant alloy during long term aging at 700â€ <sup>-</sup> °C. Journal of Alloys and Compounds, 2018, 765, 1267-1274.	2.8	15
58	Analysis of the interaction between moving $\hat{l}\pm/\hat{l}^3$ interfaces and interphase precipitated carbides during cyclic phase transformations in a Nb-containing Fe-C-Mn alloy. Acta Materialia, 2018, 158, 167-179.	3.8	19
59	The temperature dependence of high-temperature strength and deformation mechanism in a single crystal CoNi-base superalloy. Materials Science & Engineering A: Structural Materials: Properties, Microstructure and Processing, 2018, 735, 114-120.	2.6	21
60	Corrosion resistance behavior of gradient microstructure induced by punching deformation and recovery treatment on cupronickel alloy surface. Rare Metals, 2017, 36, 971-976.	3.6	2
61	Effect of Interfacial Mn Partitioning on Carbon Partitioning and Interface Migration During the Quenching and Partitioning Process. Metallurgical and Materials Transactions A: Physical Metallurgy and Materials Science, 2017, 48, 3168-3174.	1.1	16
62	An Overview of the Cyclic Partial Austenite-Ferrite Transformation Concept and Its Potential. Metallurgical and Materials Transactions A: Physical Metallurgy and Materials Science, 2017, 48, 2720-2729.	1.1	13
63	Predicting the Transition between Upper and Lower Bainite via a Gibbs Energy Balance Approach. Journal of Materials Science and Technology, 2017, 33, 1513-1521.	5.6	4
64	A cyclic austenite reversion treatment for stabilizing austenite in the medium manganese steels. Scripta Materialia, 2017, 136, 6-10.	2.6	35
65	Determination of the intrinsic α/γ interface mobility during massive transformations in interstitial free Fe-X alloys. Acta Materialia, 2017, 133, 258-268.	3.8	35
66	Effect of Cu on Nanoscale Precipitation Evolution and Mechanical Properties of a Fe–NiAl Alloy. Microscopy and Microanalysis, 2017, 23, 350-359.	0.2	10
67	Co-based alloys design based on first-principles calculations: Influence of transition metal and rare-earth alloying element on stacking fault energy. AIP Conference Proceedings, 2017, , .	0.3	4
68	Understanding cementite dissolution in pearlitic steels subjected to rolling-sliding contact loading: A combined experimental and theoretical study. Acta Materialia, 2017, 141, 193-205.	3.8	23
69	Effects of alloying elements concentrations and temperatures on the stacking fault energies of Co-based alloys by computational thermodynamic approach and first-principles calculations. Journal of Alloys and Compounds, 2017, 694, 1265-1279.	2.8	56
70	Prediction of Ar <sub>3</sub> during Very Slow Cooling in Low Alloy Steels. ISIJ International, 2016, 56, 678-684.	0.6	2
71	Effect of Mo Addition on the Transformation Stasis Phenomenon During the Isothermal Formation of Bainitic Ferrite. Metallurgical and Materials Transactions A: Physical Metallurgy and Materials Science, 2016, 47, 5670-5674.	1.1	4
72	Microstructural Evolution of a Hypoeutectoid Pearlite Steel under Rolling-sliding Contact Loading. Journal of Iron and Steel Research International, 2016, 23, 1054-1060.	1.4	21

HAO CHEN

#	Article	IF	CITATIONS
73	Phase Field Modeling of Cyclic Austenite-Ferrite Transformations in Fe-C-Mn Alloys. Metallurgical and Materials Transactions A: Physical Metallurgy and Materials Science, 2016, 47, 3873-3881.	1.1	14
74	First-principles calculations of generalized-stacking-fault-energy of Co-based alloys. Computational Materials Science, 2016, 121, 86-96.	1.4	67
75	Effect of stress-temperature coupling on gradient alloying induced by punching severe deformation. Journal of Alloys and Compounds, 2016, 662, 436-440.	2.8	4
76	The Effect of Interfacial Element Partitioning on Ferrite and Bainite Formation. Jom, 2016, 68, 1320-1328.	0.9	12
77	Microstructure evolution of a hypereutectoid pearlite steel under rolling-sliding contact loading. Materials Science & Engineering A: Structural Materials: Properties, Microstructure and Processing, 2016, 655, 50-59.	2.6	47
78	On the transition between grain boundary ferrite and bainitic ferrite in Fe–C–Mo and Fe–C–Mn alloys: The bay formation explained. Acta Materialia, 2016, 104, 62-71.	3.8	21
79	Phase-field modeling of cyclic phase transformations in low-carbon steels. Computational Materials Science, 2015, 108, 333-341.	1.4	25
80	Application of the cyclic phase transformation concept for determining the effective austenite/ferrite interface mobility. Computational Materials Science, 2014, 83, 92-100.	1.4	22
81	Predicting the Austenite Fraction After Intercritical Annealing in Lean Steels as a Function of the Initial Microstructure. Metallurgical and Materials Transactions A: Physical Metallurgy and Materials Science, 2014, 45, 1675-1679.	1.1	14
82	A general mixed-mode model for the austenite-to-ferrite transformation kinetics in Fe–C–M alloys. Acta Materialia, 2014, 72, 1-12.	3.8	86
83	Impact of Particle Size on the Non-Equilibrium Phase Transition of Lithium-Inserted Anatase TiO <sub>2</sub> . Chemistry of Materials, 2014, 26, 1608-1615.	3.2	68
84	Predicting the Effect of Mo, Ni, and Si on the Bainitic Stasis. Metallurgical and Materials Transactions A: Physical Metallurgy and Materials Science, 2014, 45, 3429-3437.	1.1	24
85	A Detailed Study of the Transformation Stasis Phenomenon during the Isothermal Bainite Transformation in Mn Based Low Alloy Steels. , 2014, , 909-917.		0
86	The effect of prior ferrite formation on bainite and martensite transformation kinetics in advanced high-strength steels. Acta Materialia, 2013, 61, 6025-6036.	3.8	74
87	In situ observation of austenite–ferrite interface migration in a lean Mn steel during cyclic partial phase transformations. Acta Materialia, 2013, 61, 2414-2424.	3.8	54
88	Analysis of ferrite growth retardation induced by local Mn enrichment in austenite created by prior interface passages. Acta Materialia, 2013, 61, 1338-1349.	3.8	36
89	Analysis of transformation stasis during the isothermal bainitic ferrite formation in Fe–C–Mn and Fe–C–Mn–Si alloys. Acta Materialia, 2013, 61, 5458-5468.	3.8	76
90	Application of interrupted cooling experiments to study the mechanism of bainitic ferrite formation in steels. Acta Materialia, 2013, 61, 4512-4523.	3.8	30

#	Article	IF	CITATIONS
91	Experimental Evidence of the Effect of Alloying Additions on the Stagnant Stage Length During Cyclic Partial Phase Transformations. Metallurgical and Materials Transactions A: Physical Metallurgy and Materials Science, 2013, 44, 5617-5621.	1.1	15
92	Application of the stagnant stage concept for monitoring Mn partitioning at the austenite-ferrite interface in the intercritical region for Fe–Mn–C alloys. Philosophical Magazine Letters, 2012, 92, 547-555.	0.5	18
93	Analysis of the stagnant stage in diffusional phase transformations starting from austenite–ferrite mixtures. Computational Materials Science, 2012, 55, 34-43.	1.4	23
94	Indirect evidence for the existence of the Mn partitioning spike during the austenite to ferrite transformation. Philosophical Magazine Letters, 2012, 92, 86-92.	0.5	24
95	Application of cyclic partial phase transformations for identifying kinetic transitions during solid-state phase transformations: Experiments and modeling. Acta Materialia, 2011, 59, 6751-6760.	3.8	71
96	Modeling of soft impingement effect during solid-state partitioning phase transformations in binary alloys. Journal of Materials Science, 2011, 46, 1328-1336.	1.7	42
97	Consideration of the growth mode in isochronal austenite-ferrite transformation of ultra-low-carbon Fe–C alloy. Applied Physics A: Materials Science and Processing, 2010, 98, 211-217.	1.1	17
98	Application of the cyclic phase transformation concept for investigating growth kinetics of solid-state partitioning phase transformations. Computational Materials Science, 2010, 49, 801-813.	1.4	27
99	A Mixed-Mode Model Considering Soft Impingement Effects for Solid-State Partitioning Phase Transformations. Solid State Phenomena, 0, 172-174, 561-566.	0.3	1
100	Interface Motion and Interface Mobility of the Partitioning Phase Transformations in Fe-Mn-C and Fe-C Alloys: A Cyclic Phase Transformation Approach. Materials Science Forum, 0, 706-709, 1367-1372.	0.3	0